# Agglomeration Mechanism of Complex Ti-Al Oxides in Liquid Ferrous Alloys Considering High-Temperature Interfacial Phenomenon

WANGZHONG MU and CHANGJI XUAN

This work presents the agglomeration mechanism of complex Ti-Al oxides in the liquid ferrous alloy. Cluster characteristics were investigated using Al and Ti/Al-complex deoxidation method in lab scale. The time-dependent size distribution, total number per volume, average size, and circularity of the clusters were quantitatively analyzed. Furthermore, high-temperature confocal laser scanning microscopy was utilized to directly observe the cluster formation of Ti-Al oxides. A capillary force model including wettability parameters was applied to compare the agglomeration capabilities of different types of non-metallic inclusions. When a low Ti is added into melt, the agglomeration of $TiO_x \cdot FeO$ liquid inclusions is one of the key factors to decrease the frequency of cluster formation. When the Al is added into melt, the heterogeneous precipitation on $TiO_x \cdot FeO$ surfaces is the main reaction process. Ti-Al oxides have lower agglomeration ability than that of $Al_2O_3$, which in turn, contribute to a low agglomeration frequency as well.

## I. INTRODUCTION

THERMODYNAMIC and kinetic aspects of Ti-Al-O system have attracted the attentions from different scientific and engineering fields. For instance, the continuous formed Ti-Al-O oxide layer on the surface of Ti-based alloys can prohibit the further oxidation of the alloy. The stability of the protective oxide films has been investigated.[1,2] Furthermore, the phase equilibria of Ti-Al-O ternary system has been evaluated by different researchers with specific aims.[3–5] A more specific application of Ti-Al-O has been provided by Mas-Guindal et al.,[6] and the synthesis of the nanostructured metastable cermets of Ti-$Al_2O_3$ has been performed through activated SHS reaction.

From the engineering application perspective, Ti-Al-O oxide is one of the most important inclusion types which should be considered in metallurgical process. Motion behaviors of inclusion particles[7–14] in a fluid or at different interfaces have great importance in such different fields as colloid chemistry, material science, and metallurgical engineering and welding.

Different types of interfacial reactions are deemed as the key driving force of particle behaviors at different interfaces.[7–15] For instance, the wettability and detachment energy are important factors that influence anisotropic particles at the liquid/liquid interfaces.[9] Moreover, it was found that the critical interfacial force to detach particles from a coagulated cluster is required to be the same as the maximum capillary force that keeps the particles at interfaces.[10] In the case of particles detaching, capillary force has been recognized as the main driving force of particle agglomeration[16–18] as well as the chain cluster deformation[12] at liquid steel/ Ar interfaces. This process has been proved by using both in-situ observations and mathematical modelings. Particle collision–coalescence in fluid is affected by such different forces[11,19] as Van der Waals force, cavity bridge force, etc. A more general description of interfacial forces has been proposed in References 20 and 21.

The application of interfacial phenomena in non-metallic particle behaviors are known as inclusion engineering[22,23] or oxide metallurgy.[24–31] In these topics, the interfacial energy is the key issue[23–25] to influence the inclusion motion and nucleation behaviors in liquid and solid steels. Among different types of oxide inclusions, Ti-Al-complex oxide[32–43] is one of the most important types since it is extensively existed in low-alloy steel grades, e.g., interstitial free (IF) steels. In most previous work, inclusion characteristics were investigated by a deoxidation sequence of first Al and followed by Ti addition (Al/Ti). Specifically, Matsuura et al.[32] investigated the inclusion evolution in IF steel with Al,

WANGZHONG MU is with the Department of Materials Science and Engineering, KTH Royal Institute of Technology, Brinellvägen 23, 100 44, Stockholm, Sweden. CHANGJI XUAN is with the Uddeholms AB (a voestalpine company), Uvedsvägen 15, 683 31, Hagfors, Sweden. Contact e-mail: xuanchangji@msn.com
Manuscript submitted May 12, 2019.
Article published online September 16, 2019.

Ti, and Al/Ti. It is reported that Ti addition can form oxide inclusions containing maximum 20 at. pct Ti due to the Ti supersaturation and local Al depletion. Meanwhile, the fraction of Ti-contained inclusions increases with an increased Ti addition amount. It is also mentioned that when Al and Ti are added simultaneously into melt, the formation of $Al_2O_3$ occurs much faster than that of Ti oxides. In addition, the morphology evolution of $Al_2O_3$ from spherical shape to polygonal shape happens within 5 minutes after Al deoxidation. Following this work, Wang *et al.*[33–35] reported more detailed investigations that are in consistent with Reference 32. Li *et al.*[36,37] further continued this series story and reported the Al-Ti-oxide inclusion evolution under isothermal heating treatment at 1300 °C. They reported that most of the homogeneous Al-Ti-oxide inclusions changed to Al-rich and Ti-rich heterogeneous inclusions after heating treatment. Furthermore, they utilized an inductive separation method to investigate the mechanism of Ti-bearing inclusion formation.[38] Besides Al/Ti deoxidation, Sun *et al.* reported the mechanism of single particle precipitation in Ti/Al-complex deoxidation.[39] Oxide inclusions with holes were observed frequently. Small $TiO_x$ particles were identified inside of the hollow holes of the $Al_2O_3$ crust inclusion. Sun *et al.* proposed that $TiO_x$ firstly forms after Ti pre-deoxidation. When Al is added subsequently, the complex layer of $Al_2O_3$-$TiO_x$ precipitates on $TiO_x$ surfaces. With the progress of reduction of $TiO_x$, iron melt can penetrate into the hollow holes. Finally, $TiO_x$ can be completely dissolved. Although the evolution of single inclusion has been described, it is still unclear regarding the inclusion agglomeration mechanism in Ti/Al-complex deoxidation. Xuan *et al.*[19] reported some plausible issues of clusters with large size. A comparison of cluster number in the Fe-10 pct Ni alloys deoxidized by Al and Ti/Al has been performed. However, the influence of different amounts of Ti/Al addition on the cluster formation has not been mentioned.

Even though tremendous work regarding Ti-Al-oxide inclusion has been reported, most of previous researches mainly focus on the evolution of single inclusion. Regarding the agglomeration of single type inclusions (*e.g.*, $Al_2O_3$), although several models[44–47] are available to simulate the population distribution, these models cannot be directly applied for the agglomeration of multiple type inclusions. Moreover, non-simulation work of complex chemical interactions among inclusions in agglomeration process has been reported in the literature. Meanwhile, almost all the post-characterization is performed in the solidified ingot samples. However, the agglomeration kinetics of Ti-Al oxide at real time in melt has not been reported.

The main motivation of this work was therefore to take insight into the mechanism of cluster formation by using Ti-Al-complex deoxidation in the ferrous alloy melt. In present work, the Fe-10 pct Ni alloy was selected. Due to its excellent mechanical and magnetic properties, Fe-Ni (= 10 to 30 pct) alloy has a wide application in different engineering fields in recent years, such as magnetic and inductive device manufacturing.[48–50] Many efforts have

been performed in previous studies.[51–55] for a better understanding of Fe-Ni alloy system. For example, Zeng presented the martensitic structure and hardness in Fe-Ni alloy.[52] Nakada observed the martensitic reversion in Fe-29 pct Ni alloy.[53] Furthermore, Zhao *et al.*[54] selected Fe-10Ni-0.1C to study the refinement mechanism of ferrite grains formed during dynamic austenite to ferrite transformation process. The selection of a 10 pct nickel addition to ferrous alloy is to decrease the austenite to ferrite transformation temperature and to slow down the kinetics of ferrite transformation. Besides the physical metallurgy perspective, the process metallurgy issue is also important. One of the most significant issues in the Fe-Ni alloy manufacturing is to control and optimize the non-metallic inclusions in melt.[55] The reason to select Fe-10Ni system is that fuzzy zone (liquid + solid) does not exist in this system, and Ni stabilizes the FCC region in a large area. See the binary Fe-Ni phase diagram (Figure 1) calculated by Thermo-Calc 2017b[56] with TCFE9 database.[57] In this case, the effect of solidification issues, *i.e.*, inclusion pushing and engulfment behavior in the solidified interface, can be excluded. The inclusion agglomeration only occurs in the liquid phase.

In this work, firstly, lab-scale Al and Ti/Al deoxidations with 0.02 pct and 0.06 pct Al additions were performed to investigate the influence of addition amount of deoxidizer on the cluster characteristics. Thereafter, high-temperature confocal laser scanning microscope (HT-CLSM) was used to observe the agglomeration of Ti-Al oxides. The attractive capillary force was also simulated to support the results of HT-CLSM. Finally, the mechanism of cluster formation in complex Ti/Al deoxidation was proposed.
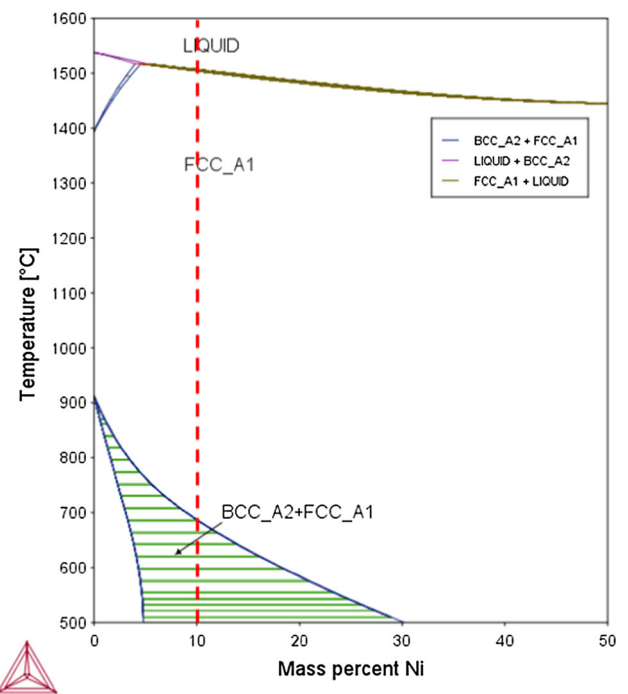


Fig. 1—Fe-Ni binary phase diagram calculated by Thermo-Calc 2017b with TCFE9 database.

## II. METHODOLOGY

### A. Experiments

#### 1. Metal sample preparation

Deoxidation experiments were performed by charging Fe-10 mass pct Ni alloy (~ 160 g) in a high-frequency induction furnace in Ar protective atmosphere. The reader is referred to Reference 19 for more details. After holding 20 minutes at 1600 °C, the alloy composition in a high-purity $Al_2O_3$ crucible is supposed to become homogeneous. The alloy was firstly deoxidized with 0.03 pct Ti addition followed by 10-second stirring with alumina rod. Different amounts of Al (0.06 or 0.02 pct) were added after holding for 1 minute at a temperature of 1600 °C. The melt was sampled after 1, 5, 10 minutes, respectively, by using quartz tube (QT) that was followed with water quenching. The liquid metal in crucible was cooled in the furnace from 1600 to 1200 °C within 15 minutes followed by water quenching. The single Al deoxidation experiments were also performed as references. The method is quite similar to that of the Ti/Al-complex deoxidation. The Al-killed melt was sampled after 1 minute and 5 minutes. The final sample after 15 minutes was quenched in the crucible.

#### 2. Inclusion particle characterization

Inclusions in metal specimens were investigated by using 3D potentiostatic electrolytic extraction (E.E.) method. The detailed experimental parameters of E.E. were described in References 55, 58, and 59. The inclusion composition was identified by using scanning electron microscope (SEM, Hitachi, S3700 type) in combination with energy dispersion spectroscopy (EDS) at different magnifications from × 1000 to × 10,000. The working acceleration voltage of SEM-EDS is between 15 and 20 kV, and the beam size of the spot analysis is approximately 2 to 3 $\mu$m. The calibration material is pure Fe ($\approx$ 99.99 pct). In addition, 2D analysis of inclusion in cross section was performed at different magnifications from × 3000 to × 10,000. The inclusion size is presented with the maximum length. The circularity and the size of inclusions were measured by using analyzer software WinROOF®. The circularity of inclusion equals 4$\pi$*(area/perimeter$^2$).

#### 3. In-situ observation by high-temperature confocal laser scanning microscopy

The agglomerations of complex Ti-Al oxides in the melt were observed in-situ using HT-CLSM. This facility used a He-Ne laser equipped with an infrared image furnace. The details of this technique have been reported elsewhere.[16–18] High-purity Ar passing through the cleaning system was used as the protection gas. In addition, thin Ti foil was wrapped around the upper outer surface of the alumina crucible to prevent re-oxidation of sample surface during heating and isothermal holding. The oxygen partial pressure ($P_{O2}$) in the off-gas during the experiment was between $10^{-19}$ and $10^{-20}$ kPa level. More details can be seen in References 16 and 17. The used alloy has the composition of Fe-0.16 C-0.15 Si-0.84 Mn-0.01 Al-0.008 Ti-0.03 S-0.016 N-0.0073 O (wt pct) containing both $Al_2O_3$ and $TiO_x$ inclusions. The reason for choosing this actual steel composition is that the authors intend to benchmark the findings of inclusion agglomeration tendency in Fe-10 pct Ni alloy in an actual multicomponent ferrous alloy. R type thermocouple is used to measure the temperature of the bottom of crucible. The actual sample surface temperature was calibrated comparing with phase transformation points of pure iron. It is found that sample surface temperature is of ± 20 °C difference with the thermocouple temperature. The steel sample was firstly heated up to 1000 °C with 100 °C/min, and subsequently to 1480 °C with 150 °C/min and to 1520 °C with 10 °C/min. Finally, it was manually heated up by an average rate of 0.5 to 1 °C/min till the steel sample is melted. After the in-situ observation, the alloy sample was directly quenched by Ar gas. It should be noted that for the application of this methodology, the inclusion agglomeration is at the steel/gas interface, and the main driving force is believed to be the capillary force, where interfacial energy as well as the wetting angle are the key issues. However, it should be pointed that this mechanism is different from the case of inclusion agglomeration in the steel matrix. This theory can be only applied to compare the confocal microscopy work of inclusion agglomeration.

### B. Theoretical Work

The capillary force model reported in References 16 through 18 was used to calculate the attraction force between Ti-Al-complex oxide and $Al_2O_3$ cluster. The physical meaning of the capillary force in this work refers to the difference of capillary pressure between the inside and the outside of the inclusion pair, which can force the two inclusions toward each other when their distance is sufficiently close. The contact angle values of $Al_2O_3$, $Ti_2O_3$, and $TiO_2$ in References 60 through 62 were used in the model calculation. This model is originally developed by Kralchevsky and co-workers,[63,64] and has been validated by offering a very reasonable agreement with the experimental data reported elsewhere.[16] The key equations of this model are summarized below.

For the different values of $L$, the capillary force, $F$, can be calculated as

$$F = \frac{d(\Delta W)}{dL} \quad [1]$$

The capillary interaction energy between two inclusion particles ($\Delta W$) can be calculated using Eq. [2]. This energy is a combination of a wetting contribution, a meniscus surface tension contribution, and a gravity contribution. Details can be seen in Reference 18.

$$\Delta W = -\pi\gamma \sum_{k=1}^{2} (Q_k h_k - Q_{k\infty} h_{k\infty})\left(1 + O\left(q^2 R_k^2\right)\right) \quad [2]$$

$$q = \sqrt{\frac{(\rho_I - \rho_{II})g}{\gamma}} \approx \sqrt{\frac{\rho_I g}{\gamma}}, \text{ where } \rho_I >> \rho_{II}, \quad [3]$$

where $\rho_I$ and $\rho_{II}$ are the densities of liquid metal (I) and Ar gas (II). q is the capillary length, defined by Eq. [3]. $\gamma$ is the surface tension of the liquid metal. g is gravity acceleration. The subscript k represents the inclusion 1 or 2 in a pair. The $O(x)$ is the zero function of the approximation. Subsequently, the capillary charges and the height differences of the meniscus, ($Q_k$ and $Q_{k\infty}$, and $h_k$ and $h_{k\infty}$) can be calculated as follows.

$$Q_k = \frac{1}{2}q^2\left(b_k^2\left(R_k - \frac{1}{3}b_k\right) - \frac{4}{3}D_k R_k^3 - r_k^3 h_k\right) \quad [4]$$

$$h_k = (\tau_k + 2\ln(1 - \exp(-2\tau_k))) - (Q_1 + Q_2)\ln(\gamma_e qa)$$
$$+ (Q_1 - Q_2)\left(A - (-1)^k\sum_{n=1}^{\infty}\frac{2}{n}\frac{\exp(-n\tau_k)\sinh n\tau_j}{\sinh n(\tau_1 + \tau_2)}\right)$$
$$[5]$$

where $j$ and $k$ = 1 and 2, $j \neq k$; $(qR_k)^2 \ll 1$. $r_k$ is capillary meniscus radius, $R_k$ is the radius of inclusion $k$, $\phi$ is the angle according to the slope of the meniscus, $b_k$ is the immersion depth, $\alpha_k$ is the contact angle between the inclusion and the liquid metal, and $L$ is the distance between the inclusion and inclusion/cluster at the interface. $\gamma_e$ is the Euler–Mascheroni constant, and a value of 1.78 is used here.[16,17] $D_k$ is the density ratio. The parameters, $a$, $A$, and $\tau_k$ are used for the simplification of Eq. [5]. Detailed equations can be seen in Reference 18.

## III. RESULTS

### A. *Morphology and Composition of Clusters in Al and Ti/Al-Complex Deoxidations*

Figure 2 shows the typical morphology of the clusters in the Fe-10 pct Ni alloy deoxidized by Al and Ti/Al. The clusters are extracted by E.E. method. In the case of Al deoxidation, the clusters have irregular morphology with low circularity. In the case of Ti/Al-complex deoxidation, the clusters are more compact and have relative higher circularity. The same phenomenon has been reported in Reference 19. Figure 3 shows SEM-EDS element mapping of the typical clusters in the Ti/Al-complex deoxidation case. Specifically,

Figure 3(a) shows the distribution of different elements on the surface of Ti-Al-oxide cluster extracted using E.E. method. It can be seen that certain zones of the cluster have pure $Al_2O_3$ phases, and some other zones have $Al_2O_3$-$TiO_x$-FeO phases. Figure 3(b) shows the mapping of the cross sectional of a typical Ti-Al-oxide cluster. Several $TiO_x$/$TiO_x$-FeO cores are covered by $Al_2O_3$ layer. It is quite difficult to directly judge whether the cores are $TiO_x$ or $TiO_x$-FeO inside the cluster due to the low resolution of the metallic element matrix. However, using Ti deoxidation method, a previous work by the present authors[65] reported that precipitation phase is $TiO_x$·FeO with 0.03 pct Ti addition. In order to get $TiO_x$ inclusions without Fe content, the Ti addition needs to be higher than 0.1 pct in melt. Since the same alloy composition and experimental method are used for alloy preparation in this work, it is reasonable to judge that the cores are $TiO_x$-FeO solid solution. In addition, the mapping result in Figure 3(a) can also validate this estimation.

### B. *Number and Size of Clusters in Al and Ti/Al-Complex Deoxidations*

Figure 4 shows the size distribution of clusters with different holding times from 1 to 15 min. The clusters in the alloys deoxidized by 0.02 pct Al, 0.06 pct Al, and 0.03 pct Ti-0.02/0.06 pct Al are systematically analyzed. In the case of 0.06 pct Al addition, the peak in the size distribution increases, while the number density in each size decreases with the increasing holding time. This phenomenon is due to the small size cluster agglomerated to form the larger one, which is easier to be removed. The same but less obvious tendency can be observed in the alloy with 0.02 pct Al addition. In the case of Ti/Al addition, the peak and the number density of each size do not change significantly except for the holding time of 15 minutes. At this condition, the number density of each size range is lower than the others with shorter holding time. No clear difference with different Al addition amounts (0.02 and 0.06 pct) after 0.03 pct Ti addition can be found. According to Figure 4(a), it is also obvious that the initial number density of the cluster depends on the deoxidizer (Al or Ti) addition amount. It is clear that the density of each
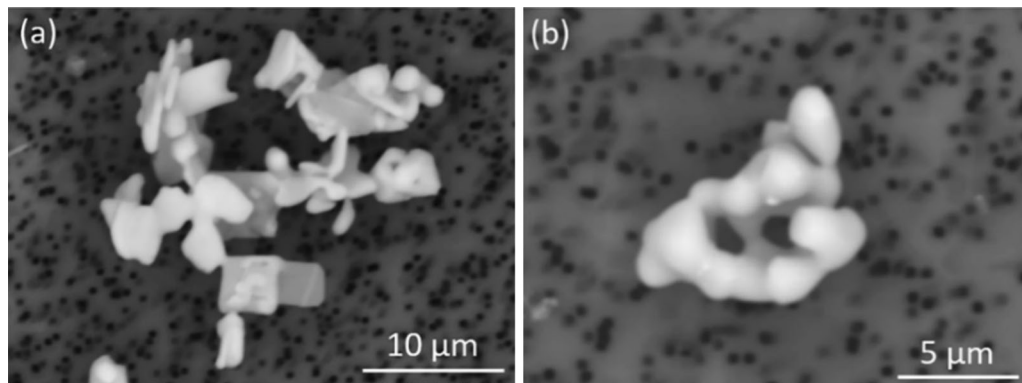


Fig. 2—Typical cluster morphology in the alloys with (*a*) Al deoxidation and (*b*) Ti/Al-complex deoxidation.
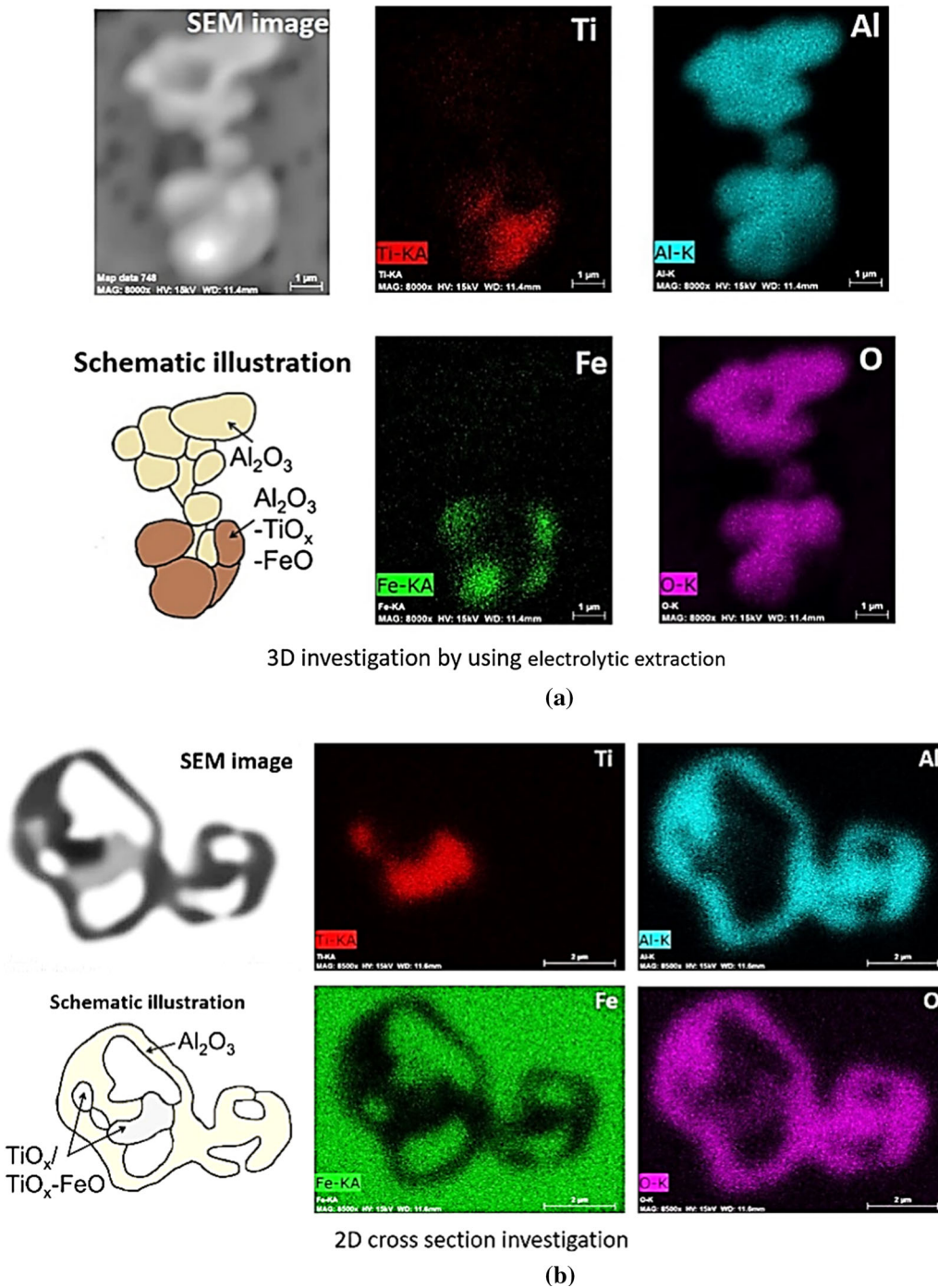
Fig. 3—Element mapping of typical cluster in Ti/Al-complex deoxidation, where (*a*) shows the cluster surface extracted by E.E., and (*b*) shows the cluster on the cross section.

size cluster decreases from 0.06 pct Al addition to 0.03 pct Ti addition, and the lowest one is the 0.02 pct Al addition. When the holding time prolongs after 1 min, the size distribution peaks of different deoxidization conditions tend to overlap, as is shown in Figure 4(b) through (d).

In order to further describe the cluster characteristics, the evolution of the total cluster number density per volume ($N_{v\text{-}c}$), average cluster size ($d_{ave.}$), and a shape factor, circularity (CF), has been summarized in Figure 5. It can be seen that the total number density decreases with the increased holding time in both the Al
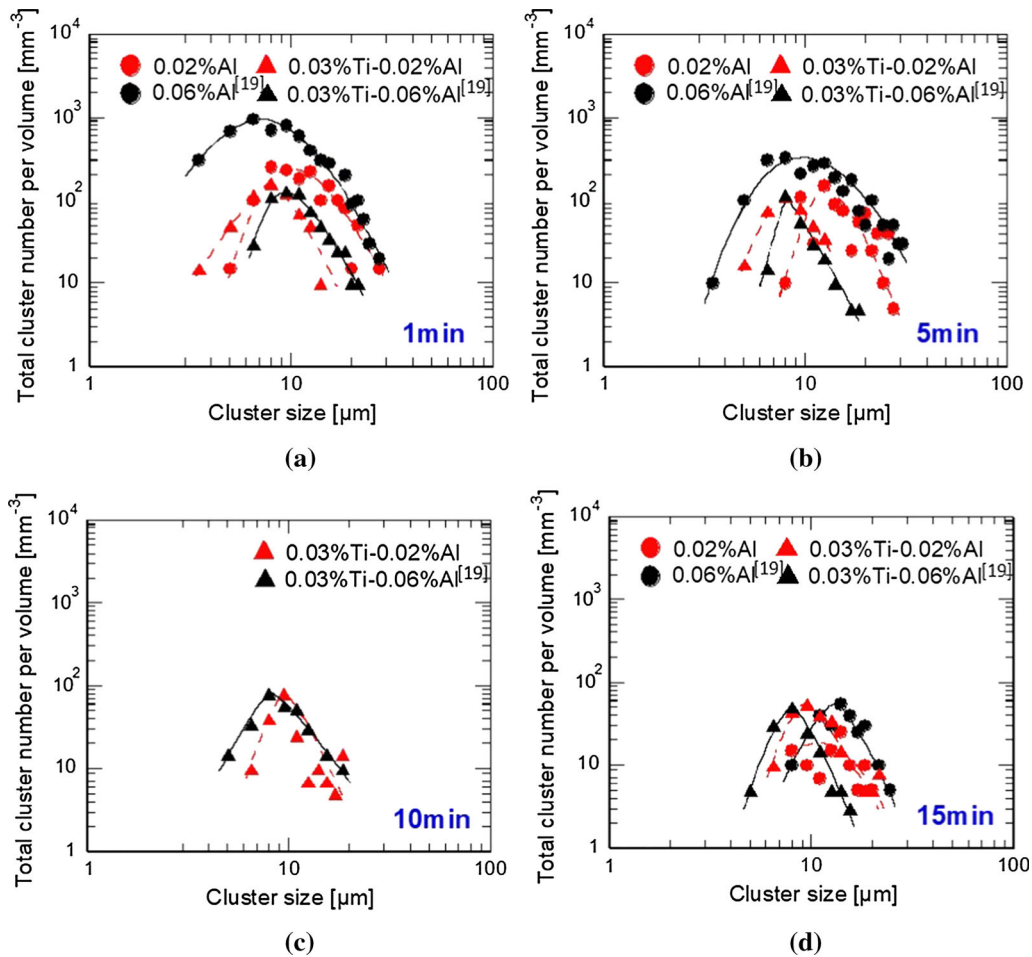
Fig. 4—Size distribution of inclusion/cluster in alloys with Al and Ti/Al addition, after a deoxidation time of (*a*) 1 min, (*b*) 5 min, (*c*) 10 min, and (*d*) 15 min.

or Ti/Al addition cases. Furthermore, it is clearly recognized that $N_{v\text{-}c}$ of 0.06 pct Al is much larger than that of 0.02 pct Al, and as a sequence, two Ti/Al cases have the lowest $N_{v\text{-}c}$. This tendency is constant at the holding time from 1 to 10 minutes. Thereafter, $N_{v\text{-}c}$ of 0.02 pct Al decreases to be the same values as that of two Ti/Al cases at the holding time of 10 minutes. $N_{v\text{-}c}$ value of 0.06 pct Al finally decreases to a level that is similar to other cases at the holding time of 15 minutes. The much higher of $N_{v\text{-}c}$ for Al addition is because that the equilibrium time of the $Al_2O_3$ formation is much faster than that of $TiO_x$. Matsuura *et al.*[32] reported that only $Al_2O_3$ was observed in the first several minutes when Al and Ti are simultaneously added into IF steel melt. Figure 5(b) shows the average cluster size changed with different holding conditions. It can be seen that the average size for all cases changes slightly. Moreover, two Al addition cases have a clear larger average size than the Ti/Al cases. Figure 5(c) shows the circularity of clusters changed with time. In the case of Al deoxidation, the average value of cluster circularity decreases from about 0.65 to 0.50 with increased Al addition from

0.02 to 0.06 pct. As for the case of Ti/Al-complex deoxidation, the circularity of clusters remains almost the same ($\approx 0.85$) when Al addition increases from 0.02 to 0.06 pct.

## IV. DISCUSSIONS

### A. *In-situ Observation of $Al_2O_3$ and Ti-Al-Complex Oxide Inclusion Agglomeration*

In order to investigate the Ti-Al cluster formation mechanism, the *in-situ* observation experiment was performed by HT-CLSM. The used ferrous alloy contains both $Al_2O_3$ and complex Ti-Al-oxide ($TiAlO_x$) inclusions. The aim of selecting this alloy is to observe cluster formation between $TiAlO_x$ and $Al_2O_3$ simultaneously. SEM-EDS chemical maps of two types of inclusions that exist in the alloy before HT-CLSM experiment are expressed in Figure 6. For the classification of these two types, around 50 inclusions in total are checked by SEM-EDS.
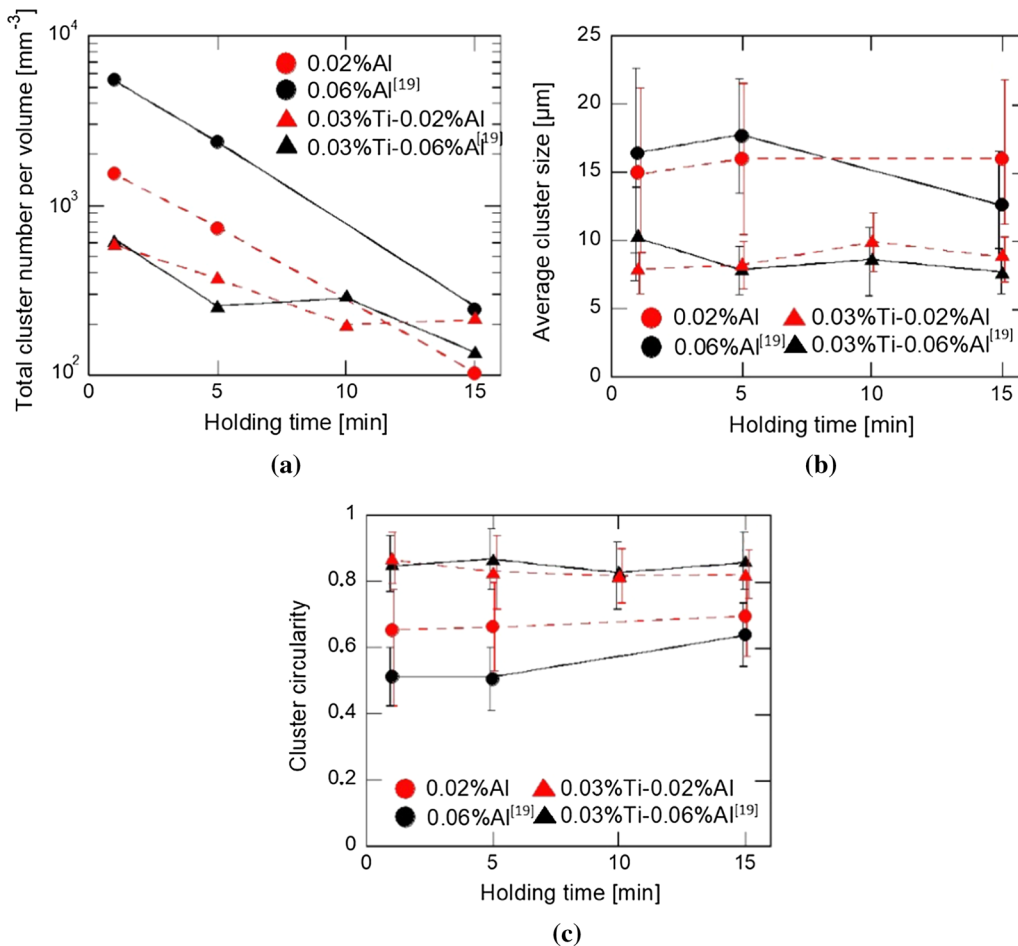
Fig. 5—(a) Total number per volume, (b) average size, and (c) circularity of inclusion/cluster in the alloy deoxidized by Al and Ti/Al with different holding times.

Typical images of *in-situ* observation of inclusion agglomeration on the surface of the liquid alloy are shown in Figure 7. Initially, small inclusions agglomerate with each other to form a large size cluster. Once the cluster is formed, it starts to absorb more inclusions. When the there is no more inclusion absorbed by the cluster, the melt was quenched in HT-CLSM, and the composition of the agglomerated cluster is characterized by SEM-EDS. The results are expressed in Figure 8. It is found that the typical agglomerated cluster is clearly $Al_2O_3$, Ti-containing oxide is not obvious found, and only trace amount of Ti can be seen in the EDS spectrum. In addition, due to the high S content (300 ppm) in steel, small amount of MnS precipitated on the cluster corner during solidification. Moreover, $TiAlO_x$ particle is only found in one cluster after checking several clusters by SEM-EDS (see the results in Appendix), which is the same as the finding by the authors.[16]

According to the different morphology of the inclusions by SEM-EDS observation (see Appendix), $TiAlO_x$ is recognized during the CLSM video, and therefore, the attractive force between $TiAlO_x$ and $Al_2O_3$ cluster is calculated based on Newton's second law, details can be seen in References 16 and 18.

$$a_i = (v_{i+1} - v_i)/\Delta t_i = (d_{i+1}/t_{i+1} - d_i/t_i)\Delta t_i \quad [6]$$

$$F_{A,i} = m_I \times a_i \times m_I/(m_I + m_{II}), \quad [7]$$

where $v_i$ and $d_i$ are the moving velocity and distance of the inclusion at each time $i$ ($t_i$), $m_I$ and $m_{II}$ are the mass of the moving inclusion I and the cluster II, $a_i$ is the acceleration of the inclusion pair at each time $t_i$, $d_i$ is the distance between two inclusions at each time $t_i$, and $\Delta t_i$ is the time interval which equals 0.15 seconds in this work. The attractive force between $TiAlO_x$ inclusion and $Al_2O_3$ cluster is shown in Figure 9. The $R_2/(R_1 + R_2)$ ratio of $TiAlO_x$-$Al_2O_3$ pair is 0.3. It is observed that attractive force increased from 1E-17 to 2E-14 N as cluster-inclusion distance decreased. Attractive forces between $Al_2O_3$ inclusion and $Al_2O_3$ cluster reported in Reference 16 are also plotted in Figure 9. For these data, the size ratio of $Al_2O_3$-$Al_2O_3$ pair, $R_2/(R_1 + R_2)$, is ranging from 0.272 to 0.372 which is quite similar to the $TiAlO_x$-$Al_2O_3$ pair, in order to make a unified comparison. It is found that attractive force between $TiAlO_x$ inclusion and $Al_2O_3$ cluster is one to two magnitudes smaller than that between $Al_2O_3$ inclusion and $Al_2O_3$ cluster. This is the reason why the majority of the cluster is $Al_2O_3$ phase
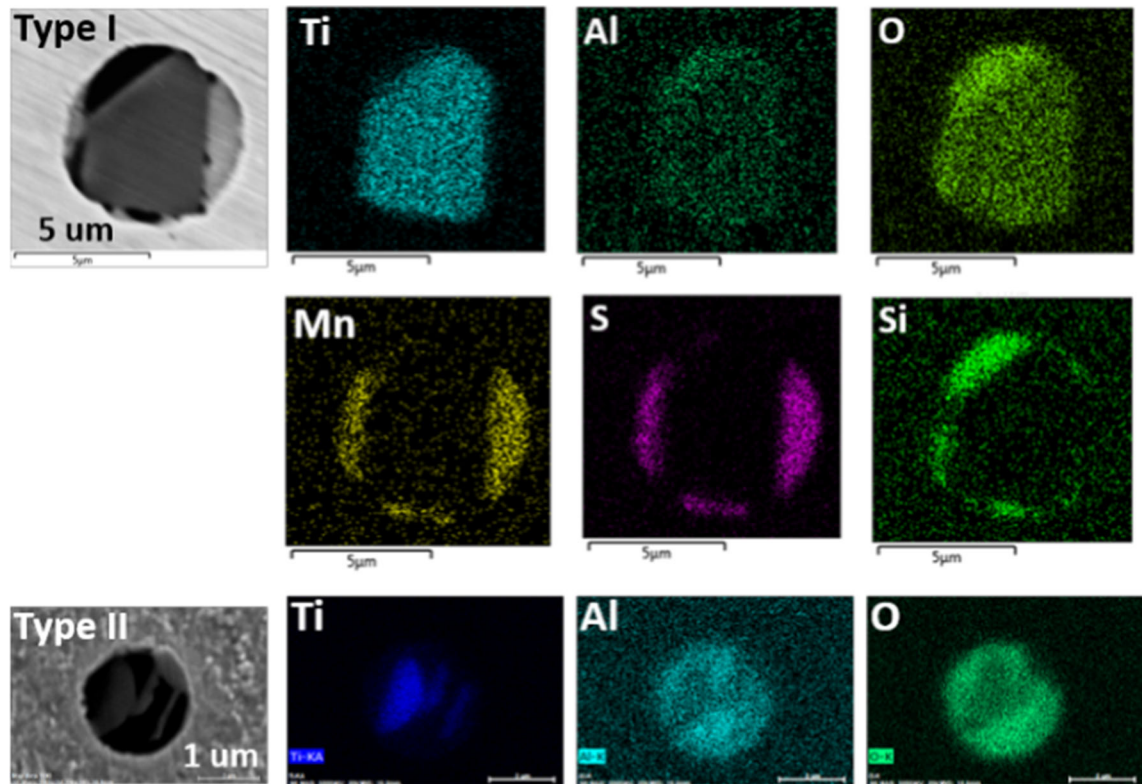
Fig. 6—SEM-EDS mapping images of two types of inclusions in the alloy before *in-situ* observation.
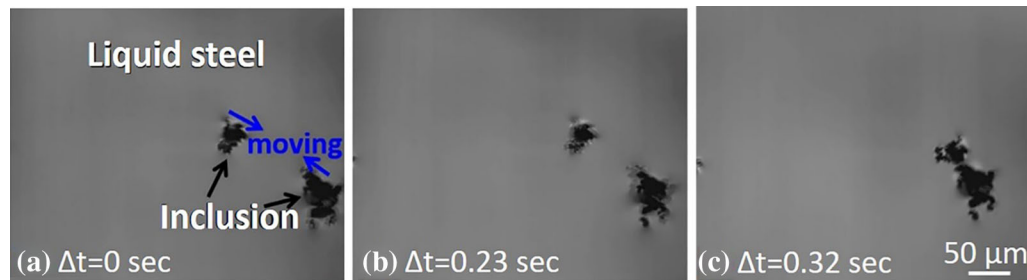


Fig. 7—HT-CLSM images of inclusion agglomeration in the liquid metal surface at the time as (*a*) $\Delta t = 0$ second, (*b*) $\Delta t = 0.23$ second, (*c*) $\Delta t = 0.32$ second.

and $TiAlO_x$ is on the local part. Moreover, this difference of attractive forces is mainly due to different contact angles between oxide and liquid alloy, surface tension of liquid alloy, and the inclusion density. The further theoretical discussion focusing on the inclusion attraction will be provided thereafter.

The contact angle values between pure iron and $Al_2O_3$, $Ti_2O_3$, and $TiO_2$ reported in open literature[60–62] are summarized in Figure 10. The contact angle was usually measured at both sides of the sample at the triple point among gas, substrate, and droplet. The initial contact angles, 137 deg for $Al_2O_3$, 124 deg for $Ti_2O_3$, and 79 deg for $TiO_2$, are used as a parameter in the capillary force model calculation. Previous work has proved that the capillary force is the key driving force for the inclusion agglomeration at the liquid metal/Ar gas interface. The calculated capillary force between

different inclusions is shown in Figure 11. It is firstly seen that all the attractive capillary force increases with the decreasing distance between inclusion and cluster at the metal/gas interface. Furthermore, the attractive force of $Al_2O_3$ is slightly higher than that of $Ti_2O_3$, and much larger than that of $TiO_2$. In our previous study,[65] the agglomeration affinity of $Al_2O_3$ and Ti oxides in steel matrix was calculated as well. The agglomeration degree of $Al_2O_3$ is stronger than that of Ti oxides in liquid steel. This tendency is a sum of the parametric influence among inclusion density, contact angle between the inclusion and the metal, and the metal surface tension. The attraction of $TiAlO_x$ is not able to provide directly due to the lack of physical parameters, *e.g.*, contact angle and interfacial tension between inclusion and metal. However, it can be postulated between $Al_2O_3$ and $TiO_2$. This estimation is made
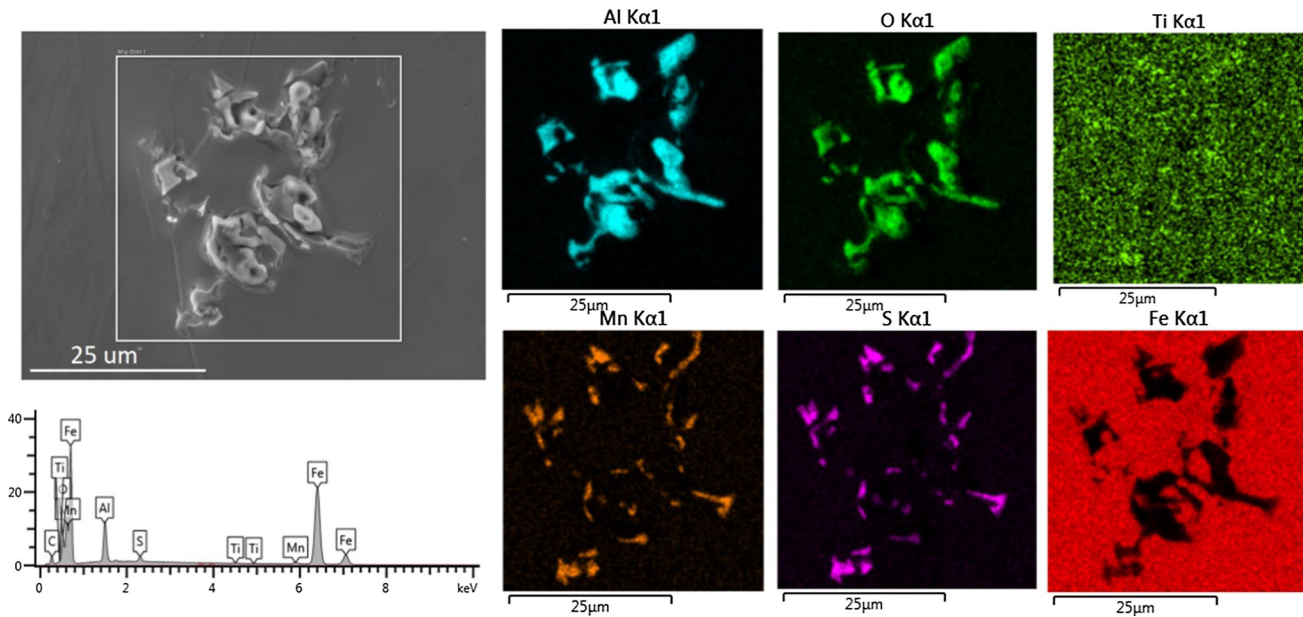
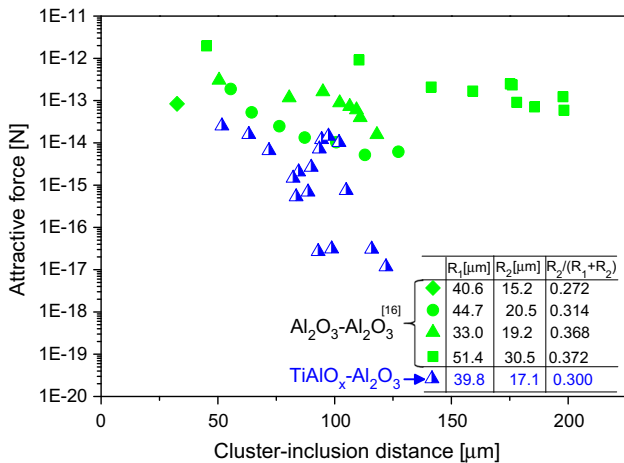Fig. 8—SEM-EDS spectrum and element mapping of typical agglomerated cluster.



Fig. 9—Comparison of attractive force between TiAlO$_x$-Al$_2$O$_3$ and Al$_2$O$_3$-Al$_2$O$_3$ inclusion-cluster pairs.



Fig. 10—Contact angle between pure iron and various oxides with different measuring times.

according to the parametric influence tendency reported in Reference 17. Based on both *in-situ* experimental and theoretical studies, Al$_2$O$_3$ has a larger agglomeration tendency than TiAlO$_x$ and Ti oxides.

### B. Agglomeration Mechanism of Inclusions in Ti/Al-Complex Deoxidation

Based on the above-mentioned experimental and theoretical analysis, the agglomeration mechanism of inclusions in Ti/Al-complex deoxidation in this work is given below:

Step 1 (Ti addition): When Ti addition is lower than 0.03 pct in melt, which corresponds to a value below the equilibrium line,[65] TiO$_x$·FeO solid solutions instead of TiO$_x$ tend to be precipitated. Due to the low melting point of TiO$_x$·FeO solid solutions,[65] the precipitated
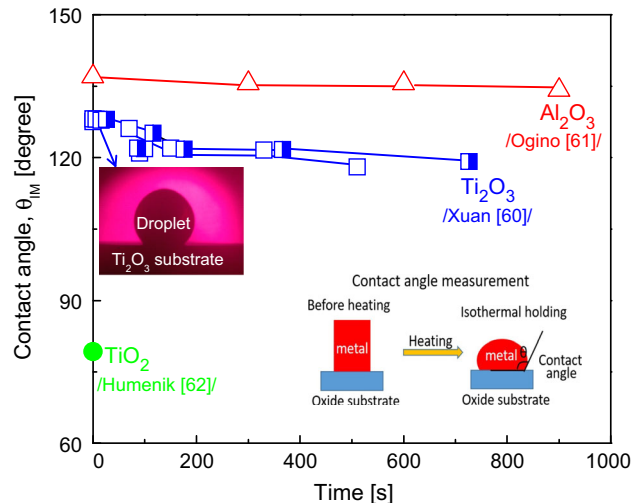
inclusions are in liquid state at temperature 1600 °C. As liquid inclusions coagulate with each other, new single inclusions with larger size can be formed. Since the turbulent influence has been avoided in deoxidation experiments, the break-up processes of liquid inclusions by turbulent flow can be negligible. The formation of solid cluster does not occur at this stage after Ti addition.

Step 2 (Al addition): When Al is added into the melt, the TiO$_x$·FeO liquid inclusions are reduced by Al, which, in turn, lead to Al$_2$O$_3$ or Al$_2$O$_3$·TiO$_x$·FeO or Al$_2$O$_3$·TiO$_x$ layer precipitations, as shown in Eqs. (8) through (10). The layer precipitations change the agglomeration behaviors. In this case, the formation of solid cluster through agglomerations can occur. It needs to be mentioned that due to the strong oxygen affinity of Al,
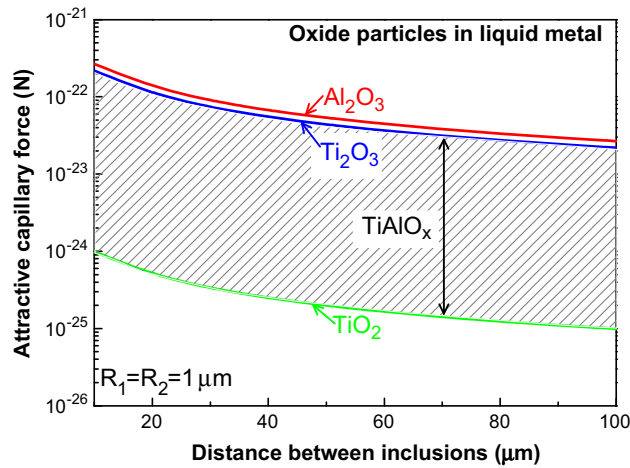
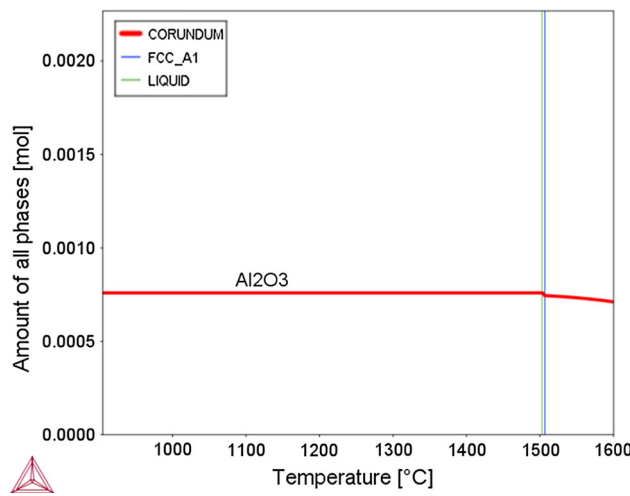Fig. 11—Comparison of calculated capillary force between different oxides at the surface of liquid metal.
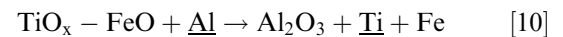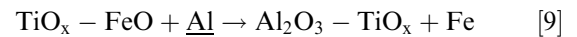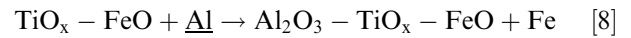


Fig. 12—Equilibrium calculation of stable inclusion precipitation in Fe-Ni-Ti-Al-O system at different temperatures.
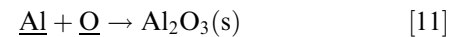
the formation of $Al_2O_3$ in melt simultaneously occurs through the Reaction (2) in Eq. [11]. It is obvious that the inclusion types in melt become complicated after the Al addition. The agglomeration frequency of Ti-Al oxides is lower than that of $Al_2O_3$ according to the *in-situ* observations and attractive force simulation in Section IV–A. Thus, the cluster formation degree in Ti/Al-complex deoxidation should be smaller than Al deoxidation if the layers of most inclusions are Ti-Al oxides instead of $Al_2O_3$. Based on Al deoxidation experiments in Section III–B, the cluster number has big increase ($\approx$ 3.5 times) at holding time of 1 minute as the amount of Al addition increases from 0.02 up to 0.06 pct. However, in the case of Ti/Al-complex deoxidation experiments, the cluster number remains almost the same even though the addition amount of Al has been increased from 0.02 to 0.06 pct (see Figure 7(a)). These results indicate that Reaction (1) is the dominant reaction instead of Reaction (2) in Ti/Al-complex deoxidation. Another reason of lower cluster formation

in the Ti/Al-complex deoxidation than that of the Al deoxidation is that the single inclusion number in melt has decreased through liquid inclusion agglomerations at Step 1. A decreased number of single inclusions can decrease the agglomeration frequency. Figure 12. shows the equilibrium calculation of stable inclusion precipitation using Thermo-Calc 2017b[56] with TCFE9 database[57] at different temperatures. The stable inclusion phase at equilibrium state is $Al_2O_3$. It means that the condition in this work has not arrived at the equilibrium state. The continuous reactions of Reaction (1) can occur until all the Ti content in inclusions is reduced by dissolved Al in liquid steel.

Reaction (1):

$$TiO_x - FeO + \underline{Al} \rightarrow Al_2O_3 - TiO_x - FeO + Fe \quad [8]$$

$$TiO_x - FeO + \underline{Al} \rightarrow Al_2O_3 - TiO_x + Fe \quad [9]$$

$$TiO_x - FeO + \underline{Al} \rightarrow Al_2O_3 + \underline{Ti} + Fe \quad [10]$$

Reaction (2):

$$\underline{Al} + \underline{O} \rightarrow Al_2O_3(s) \quad [11]$$

It has been well known that $Al_2O_3$, Ti oxides, and complex Ti-Al oxides could cause nozzle clogging in the process of continuous casting. The formation of $Al_2O_3$ cannot be avoided in single Al deoxidation. As for the case of Ti oxides, previous study[65] reported that the cluster formation through the agglomeration of single inclusions also occurs as relative high amount of Ti is added into liquid steel. On the other hand, when the Ti addition is lower than certain amount, the liquid Ti-oxide inclusions instead of solid inclusions can precipitate, and the cluster formation cannot occur. Since the oxygen affinity of Ti is much weaker than that of Al, the complex Ti-Al deoxidation can be suggested. Based on the above-mentioned analysis in current study, a small amount of Ti can be added firstly so as to bind dissolved oxygen in liquid steel and prevent solid cluster formation. After that, the addition of Al can further decrease the oxygen content in steel. Since the Ti-oxide inclusions have already precipitated, the heterogeneous reaction between Ti oxides and dissolved Al can effectively control the increase of inclusions. Moreover, due to the complex deoxidations, the morphology of clusters has a higher circularity than that in single Al deoxidation. These changes provide good potential to decrease nozzle clogging.

## V. CONCLUSIONS

The focus of the present work is the agglomeration mechanism of complex Ti-Al oxides in the ferrous alloy melt by Ti/Al deoxidation. The important conclusions can be drawn. The number density and average size of cluster in the Ti/Al-case is much smaller than that in the Al case during the first 5 minutes. When the time increases up to 15 minutes, the difference of these two cases becomes smaller. This tendency has been proved by both 0.02 and 0.06 pct Al addition cases after 0.03 pct

Ti addition. When a low Ti is firstly added into melt, the agglomeration of $TiO_x$-FeO liquid inclusions is one of the key factors to decrease the frequency of cluster formation. When the Al is added into melt, the heterogeneous precipitation on $TiO_x$-FeO surfaces is the main reaction process. Ti-Al oxides have lower agglomeration ability than that of $Al_2O_3$, which, in turn, contribute to a low agglomeration frequency.

## APPENDIX

See Figure A1.

## REFERENCES

1. A. Rahmel and P.J. Spencer: *Oxid. Metals*, 1991, vol. 35, pp. 53–68.
2. K.L. Luthra: *Oxid. Metals*, 1991, vol. 36, pp. 475–490.
3. B.J. Lee and N. Saunders: *Z. Metall*, 1997, vol. 88, pp. 152–61.
4. S. Das: *J. Ph. Eq.*, 2002, vol. 23, pp. 525–36.
5. H.J. Seifert, A. Kussmaul, and F. Aldinger: *J. Alloys Compd.*, 2001, vol. 317, pp. 19–25.
6. M.J. Mas-Guindal, E. Benko, and M.A. Rodriguez: *J. Alloys Compd*, 2008, vol. 454, pp. 352–58.
7. I. Bellemans, E.D. Wilde, N. Moelans, and K. Verbeken: *Ad. Colloid Interface Sci.*, 2018, vol. 255, pp. 47–63.
8. A.P. Weber and S.K. Friedlander: *J. Aerosol Sci.*, 1997, vol. 28, pp. 179–192.
9. T.G. Anjali and M.G. Basavaraj: *J. Colloid Interface Sci.*, 2016, vol. 478, pp. 63–71.
10. N. Sinn, M. Alishahi, and S. Hardt: *J. Colloid Interface Sci.*, 2015, vol. 458, pp. 62–68.
11. C.J. Xuan, A.V. Karasev, P.G. Jönsson, and K. Nakajima: *Steel Res. Int.*, 2017, vol. 88, p. 1600090.
12. W. Mu, N. Dogan, and K.S. Coley: *J. Mater Sci.*, 2018, vol. 53, pp. 13203–13215.
13. W. Mu, P.G. Jönsson, and K. Nakajima: *High Temp. Mater. Processes*, 2017, vol. 36, pp. 309–325.
14. W. Mu, P.G. Jönsson, and K. Nakajima: *ISIJ Int.*, 2014, vol. 54, pp. 2907–2916.
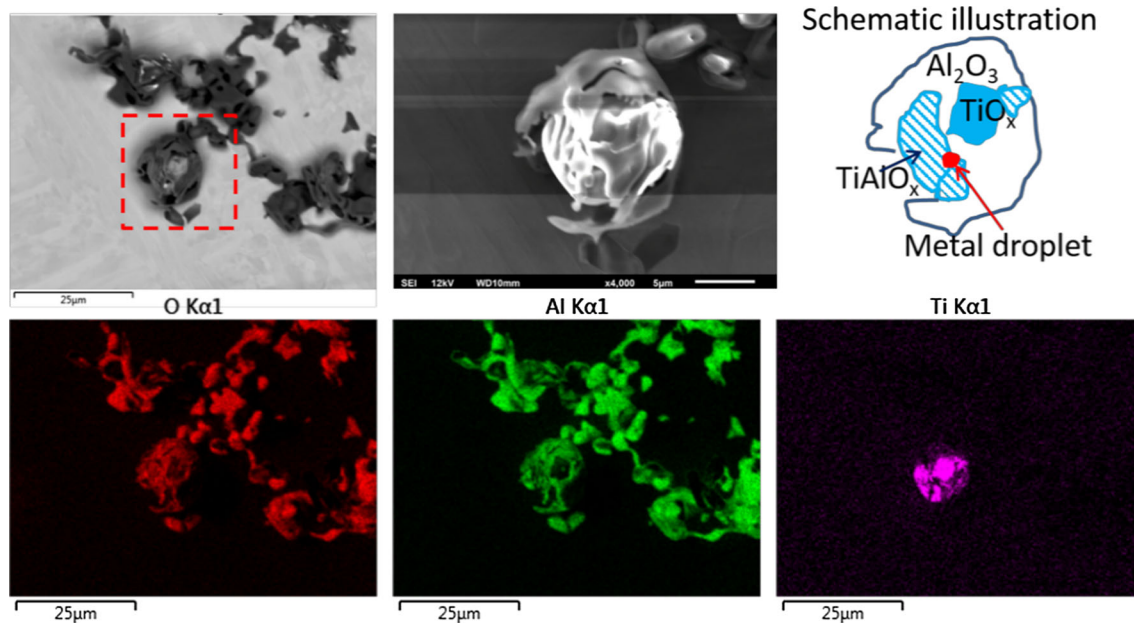
Fig. A1—SEM-EDS element mapping images of $Al_2O_3$ and $TiAlO_x$ in one agglomerated cluster.

15. E. Dickinson and L. Eriksson: *Adv. Colloid Interface Sci.*, 1991, vol. 34, pp. 1–29.
16. W. Mu, N. Dogan, and K.S. Coley: *Metall. Mater. Trans. B*, 2017, vol. 48B, pp. 2379–88.
17. W. Mu, N. Dogan, and K.S. Coley: *Metall. Mater. Trans. B*, 2017, vol. 48B, pp. 2092–2103.
18. W. Mu, N. Dogan, and K.S. Coley: *JOM*, 2018, vol. 70, pp. 1199–1209.
19. C. Xuan, A.V. Karasev, and P.G. Jönsson: *ISIJ Int.*, 2016, vol. 56, pp. 1204–09.
20. G. Kaptay: *Adv. Colloid Interface Sci.*, 2018, vol. 256, pp. 163–92.
21. G. Kaptay: *J. Mater. Sci.*, 2005, vol. 40, pp. 2125–31.
22. O. Wijk: Inclusion Engineering. Proc. 7th Int. Conf. Refining Process (SCANINJECT VII), Luleå, Sweden, 1995, pp. 35–67.
23. L. Holappa and O. Wijk: *Inclusion Engineering. Treatise on Process Metallurgy: Industrial Processes*, Elsevier, New York, 2014, pp. 347–72.
24. W. Mu, P.G. Jönsson, and K. Nakajima: *J. Mater. Sci.*, 2016, vol. 51, pp. 2168–80.
25. K.J. Malmberg, H. Shibata, S.Y. Kitamura, P.G. Jönsson, S. Nabeshima, and Y. Kishimoto: *J. Mater. Sci.*, 2010, vol. 45, pp. 2157–64.
26. J. Janis, K. Nakajima, A. Karasev, H. Shibata, and P.G. Jönsson: *J. Mater. Sci.*, 2010, vol. 45, pp. 2233–38.
27. D. Zhang, Y. Shintaku, S. Suzuki, and Y.I. Komizo: *J. Mater. Sci.*, 2012, vol. 47, pp. 5524–28.
28. X.L. Wan, R. Wei, L. Cheng, M. Enomoto, and Y. Adachi: *J. Mater. Sci.*, 2013, vol. 48, pp. 4345–55.
29. W. Mu, H. Shibata, P. Hedström, P.G. Jönsson, and K. Nakajima: *Metall. Mater. Trans. B*, 2016, vol. 47B, pp. 2133–47.
30. C. Xuan, M. Mu, Z.I. Olano, P.G. Jönsson, and K. Nakajima: *Steel Res. Int.*, 2016, vol. 87, pp. 911–20.
31. W. Mu, H. Shibata, P. Hedström, P.G. Jönsson, and K. Nakajima: *Steel Res. Int.*, 2016, vol. 87, pp. 10–14.
32. H. Matsuura, C. Wang, G. Wen, and S. Sridhar: *ISIJ Int.*, 2007, vol. 47, pp. 1265–74.
33. C. Wang, N.T. Nuhfer, and S. Sridhar: *Metall. Mater. Trans. B*, 2009, vol. 40B, pp. 1005–21.
34. C. Wang, N.T. Nuhfer, and S. Sridhar: *Metall. Mater. Trans. B*, 2009, vol. 40B, pp. 1022–34.
35. C. Wang, N.T. Nuhfer, and S. Sridhar: *Metall. Mater. Trans. B*, 2010, vol. 41B, pp. 1084–94.
36. M. Li, H. Matsuura, and F. Tsukihashi: *Metall. Mater. Trans. B*, 2017, vol. 48B, pp. 1915–23.
37. M. Li, H. Matsuura and F. Tsukihashi: Metall. Mater. Trans. A, 2018. https://doi.org/10.1007/s11661-018-5015-3.
38. M. Li, H. Matsuura, and F. Tsukihashi: *Mater. Charact.*, 2018, vol. 136, pp. 358–66.
39. M.K. Sun, I.H. Jung, and H.G. Lee: *Met. Mater. Int.*, 2008, vol. 14, pp. 791–98.
40. I.H. Jung, S.A. Decterov, and A.D. Pelton: *ISIJ Int.*, 2004, vol. 44, pp. 527–36.
41. S. A. Decterov, I. -H. Jung, E. Jak. Y.-B. Kang, P. Hayes and A. D. Pelton: Proc. 7th Int. Conf. Molten Slags, Fluxes and Salts, Café Town, South Africa, 2004, pp. 839-850.
42. F. Ruby-Meyer, J. Lehmann, and H. Gaye: *Scand. J. Metall.*, 2000, vol. 29, pp. 206–12.
43. W. Choi, H. Matsuura, and F. Tsukihashi: *ISIJ Int.*, 2011, vol. 51, pp. 1951–56.
44. T. Nakaoka, S. Taniguchi, K. Matsumoto, and S.T. Johansen: *ISIJ Int.*, 2001, vol. 41, pp. 1103–11.
45. H. Lei, L. Wang, Z. Wu, and J. Fan: *ISIJ Int.*, 2002, vol. 42, pp. 717–25.
46. H. Lei, K. Nakajima, and J.-C. He: *ISIJ Int.*, 2010, vol. 50, pp. 1735–45.
47. H. Arai, K. Matsumoto, S. Shimasaki, and S. Taniguchi: *ISIJ Int.*, 2009, vol. 49, pp. 965–74.
48. R. Hamzaoui, O. Elkedim, N. Fenineche, E. Gaffet, and J. Craven: *Mater. Sci. Eng. A*, 2003, vol. 360, pp. 299–305.
49. R. Hamzaoui, O. Elkedim, and E. Gaffet: *Mater. Sci. Eng. A*, 2004, vol. 381, pp. 363–71.
50. R. Hamzaoui and O. Elkedim: *J. Alloys Compd.*, 2013, vol. 573, pp. 157–62.
51. J.F. Li, W.Q. Jie, G.C. Yang, and Y.H. Zhou: *Acta Mater.*, 2002, vol. 50, pp. 1797–1807.
52. T. Zeng: J. Alloys Compd. 2019. https://doi.org/10.1016/j.jallcom.2017.08.285.
53. N. Nakada: *Mater. Lett.*, 2017, vol. 187, pp. 166–69.
54. L. Zhao, N. Park, Y. Tian, A. Shibata, and N. Tsuji: Adv. Eng. Mater., vol. 19, 2017. https://doi.org/10.1002/adem.201600778.
55. A.V. Karasev and H. Suito: *ISIJ Int.*, 2008, vol. 48, pp. 1507–16.
56. J.-O. Andersson, T. Helander, L. Höglund, P. Shi, and B. Sundman: *CALPHAD*, 2002, vol. 26, pp. 273–312.
57. TCFE9: TCS Steels/Fe-Alloys Database Version 9.0, Thermo-Calc Software AB, Sweden, 2017.
58. A.V. Karasev and H. Suito: *ISIJ Int.*, 2009, vol. 49, pp. 229–38.
59. H. Suito, A.V. Karasev, M. Hamada, R. Inoue, and K. Nakajima: *ISIJ Int.*, 2011, vol. 51, pp. 1151–62.
60. C. Xuan, H. Shibata, S. Sukenaga, P.G. Jönsson, and K. Nakajima: *ISIJ Int.*, 2015, vol. 55, pp. 1882–90.
61. K. Ogino, K. Nogi, and Y. Koshida: *Tetsu-to-Hagané*, 1973, vol. 59, pp. 1380–87.
62. J.M. Humenik and W.D. Kingery: *J. Am. Ceram. Soc.*, 1954, vol. 37, pp. 18–23.
63. P.A. Kralchevsky, V.N. Paunov, N.D. Denkov, I.B. Ivanov, and K. Nagayama: *J. Colloid Interface Sci.*, 1993, vol. 155, pp. 420–37.
64. V.N. Paunov, P.A. Kralchevsky, N.D. Denkov, and K. Nagayama: *J. Colloid Interface Sci.*, 1993, vol. 157, pp. 100–112.
65. C. J. Xuan and W. Mu: J. Mater. Sci. 2019. https://doi.org/10.1007/s10853-019-03458-z.